Experimental Laboratory Investigation on the Threshold of Soil Saturation and Profile on Slopes Prone to Extended Rains

Emmanuel B. Barbas[1*] and Glen A. Lorenzo[2]
[1]College of Engineering and Technology
Mindanao State University – Iligan Institute of Technology
Iligan City, 9200 Philippines
*emmb_123@rocketmail.com

[2]Civil Engineering Department
Mindanao State University – Marawi
Marawi City, 9700 Philippines

Abstract

The increase in the degree of soil saturation by rainwater infiltration is detrimental to the stability of slopes. For an accurate assessment of the potential triggering of rainfall-induced slope instabilities, the use of analytical assessment methods must be complemented with more precise information regarding the dynamic saturation behavior of the investigated soil. To obtain such soil-specific data, this study conducted a series of laboratory saturation simulations by exposing the variably sloped soil sample to artificial rains of moderate and typhoon-patterned intensities. The recorded data were consolidated to profile the temporal saturation responses of the soil, provide empirical equations for estimation of the normal movement of the infiltration front, and determine the saturation threshold of the tested soil. Based on the results, it was found out that the wettest possible soil state could be attained under partially saturated conditions but only for gentle slopes of up to 20°. The fully saturated zone originated at the bottom as opposed to the wetting front concept. For steeper slopes of 30° and above, surface runoff was more dominant that the infiltrated water could barely increase the soil moisture content at a depth of 0.626 m by less than 5%. High saturation thresholds were observed at the bottom (0.626 m depth) at values ranging from 83.7 to 99.7%.

1. Introduction

Slope instabilities are common natural phenomena that pose threats to life security, natural resource integrity, agricultural productivity, and infrastructural accessibility. Since slope failures occur frequently during or after heavy rainfall, pieces of literature widely recognize rainfall as the predominant trigger for such phenomena (Berti *et al*., 2012; White and Singham, 2012; Shao *et al*., 2015). Rainfall seems to dominate the temporal occurrences of instabilities, while some soil-based features (slope geometry, soil properties, vegetal cover, and tension cracks) dictate the spatial distributions. In other words, slope instabilities result from critical interactions between the hydrological and mechanical processes in soils (Sorbino and Nicotera, 2012). In principle, an increase in the degree of soil saturation due to rainwater infiltration causes both soil shear strength reduction and soil weight increase. These dual effects tend to progress concurrently during or very shortly after a rainfall event. With time, a soil stress condition may develop where the available shear strength is no longer sufficient to equilibrate the action of the destabilizing stress mostly due to soil weight. This stress state may occur before or upon reaching the soil saturation threshold. At this stage, slope instability may ultimately result.

As mitigation measures, the majority of research efforts have been focused on developing models for forecasting the spatiotemporal occurrences of the aforementioned hazards. Many models such as rainfall threshold models tend to correlate slope instability initiations to rainfall events, though there is no direct relationship between the two (Berti *et al*., 2012). Some authors developed sophisticated analytical forecasting models that are grounded on the effective stress concept (Muntohar and Liao, 2008; Montrasio and Valentino, 2016). These methods are more generic in terms of applicability except that their accuracy is highly reliant on how well the degree of soil saturation or soil moisture is quantified for certain geological and meteorological settings. Accordingly, the improvement and eventual adoption of the analytical methods will normally require a site-specific soil moisture parameter. Hence, this parameter is a necessity for an accurate assessment of the potential triggering of slope instabilities.

So far, the approaches employed in determining soil moisture as a hydrological variable for modeling of slope instability mechanism vary from purely mathematical derivations, empirical correlations, to real-time field measurements using sensors. Among the mathematical methods, the Green-

Ampt (Green and Ampt, 1911) and Richards' (Richards, 1931) infiltration equations are widely used. The Green-Ampt solution was originally formulated for horizontal soil surfaces and it was extended by Chen and Young (2006) for application to sloped surfaces. However, no enhancements were made to account for the variations in the initial soil moisture distribution, and the adopted "wetting front" concept has not been moderated to provide a more realistic soil moisture approximation behind the wetting front line. The initial moisture profile in most field soils is rarely uniform due to boundary influence, water draining, and evaporation. Also, field observations (Valentino *et al*., 2011) tend to deviate from the wetting front concept. Thus, the Green-Ampt concept still has to be substantiated with more enhancements for its general applicability. On the other hand, Richards' solution is more rigorous but does not have a closed-form solution. Its high non-linearity requires a huge amount of computational effort for solution, which, in certain cases, yields unreliable results (Farthing and Ogden, 2017).

Other methods were also explored for the possibility of formulating empirical soil moisture models based on climate data such as air temperature and precipitation with very minimal information required regarding the soil properties (Montrasio *et al*., 2010; Valentino *et al*., 2011; Bordoni *et al*., 2018). These models are simple in principle except that their calibrations require long records of field soil moisture observations, which may not be readily available. The advent of electronic sensors has advanced ground instrumentation techniques. Nonetheless, these approaches traditionally provide only point measurements (Dorigo *et al*., 2013). Direct field instrumentations may not be very practical because they are naturally time-consuming and expensive to conduct. For efficient characterizations of the hydrological responses of soils with respect to the highly variable natural settings, one should have control over the influencing factors, especially the slope angle and rainfall intensity and duration. In this respect, the laboratory method may be the best option.

In this paper, a series of laboratory soil saturation simulations were performed to provide precise soil-specific information on the saturation behavior of the investigated soil. Specifically, the experiments were conducted to model the effects of the time and intensity of rainfall as well as of the slope angles of ground surface on the threshold and profile of soil saturation responses.

2. Methodology

2.1 Study Area and Field Sampling

The study area was located in the barangay of New Kidapawan, Kibawe, Bukidnon, Philippines (7° 33' 24.12" N, 124° 55' 18.12" E). The climate falls under the fourth type of intermediate B type that is characterized by no very pronounced maximum rain period and no dry seasons. The rainy season is from March to October; and the months of January, February, November, and December show a reasonable regularity or no effective rainfall. From a morphological point of view, the terrain is characterized by predominantly mountainous landscapes of slopes up to 68°. The soil sample (1.5 cu. m.) was collected from a steep stretching slope of 40°. In situ samplings for bulk density and moisture content were conducted through thin-walled tubes for compaction replication in the laboratory.

2.2 Experimental Setup

The experiment arrangement (Figure 1) had three components consisting of soil tank, rainfall simulators, and soil moisture sensor system. The soil tank was made of impermeable steel plates on a rigid steel frame with interior surfaces finished with grit 36 sandpapers, except for the filter-finished perforated end drainage. It has an interior dimension of 1 m width, 2 m length, and 0.7 m depth. Surface slope variations were possible through lifting on one end via a chain block.

The rainfall simulator consisted of 16 (eight for each intensity) pressurized water sprinklers that were oriented almost vertical, equally distributed along the longitudinal direction, and placed 1.78 m above the soil tank. Each rainfall intensity required different flow pressure, nozzle head adjustments, and separate water supply lines. There were four vertically oriented and spaced, low-cost EC-5 volumetric soil moisture sensors connected to a compatible data logger (EM 50). The logger was set to read and record soil moisture contents every two-minute time-lapse during each test run. A total of 18 test runs were performed under a controlled profile of initial soil moistures (θ_i). Each test was assigned with a unique pair slope angle (α) ranging from 0° to 40°, and rainfall intensity (r) of 30.2 and 50 mm/h.
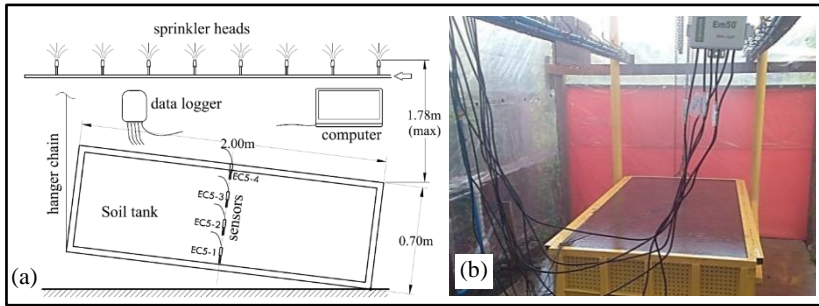
Figure 1. The Experiment Setup – schematic diagram (a) and
actual photo taken during pre-saturation stage (b)

Due to time constraint, (θ_i) was selected to represent a two-day long-duration
rainfall resulting in a profile shown in Table 1. The variations in α was fixed
to 5°. The test simulation terminates after verifying the attainment of steady-
state maximum soil saturation (referred to in this study as saturation
thresholds) for all sensors.

Table 1. Initial moisture and instrumentation profiles

Depth (m)	Initial volumetric soil moisture content (θ_i in %)	Sensor mark	Sensor height from floor (m)
0.075	47.5 ± 5%	EC5-4	0.625
0.258	50.5 ± 5%	EC5-3	0.442
0.442	54.6 ± 5%	EC5-2	0.258
0.626	56.0 ± 5%	EC5-1	0.074

2.3 Soil Compaction and Instrument Calibrations

The moisture content of the sample was determined before actual compaction
for estimation of the compaction effort required to replicate the field dry
density. The compaction was done every 0.10 m lift using a motorized plate
compactor with a rated angular speed of 1,720 revolutions per minute. This
was done during night time to avoid significant moisture loss from evaporation
that could adversely affect the actual density of the packed soil. Moisture and
tube samplings were performed at different depths to evaluate the attainment
of the desired soil dry density. The actual dry density of the compacted soil of
884.05 kg/m^3 was within the range of the field values.

Laboratory experiments involving the use of low-cost EC-5 soil moisture sensors can be carried out by adopting the generic factory calibration (Wu *et al*., 2017; Ebel *et al*., 2018; Schilirò *et al*., 2019) or by performing user-specified (soil-specific) calibration for further accuracy improvement (Huang and Yuin, 2010; Yu *et al*., 2018). In this study, the generic sensor calibration with a rated error of ± 3% was adopted (Decagon Devices, 2018) since soil-specific calibrations have shown to improve the accuracy of the device by only 1 to 2% (Huang and Yuin, 2010; Yu *et al*., 2018).

There is a general lack of standards as to the proper design of rainfall simulators (Lora *et al*., 2016). In this experiment, the authors only calibrated the intensity and distribution uniformity of the raindrops using 21 rain gauges. The distribution uniformity was evaluated using the coefficient of uniformity (*CU*) method of Christiansen (1942) in which an 80% value is rated a satisfactory performance. The size and kinetic energy of the raindrops were proportioned appropriately for laboratory scale to avoid excessive surficial erosion. The calibrated 50 and 30.2 mm/h rainfall intensities had *CU*'s of 86 and 85%, respectively. The 50 mm/h intensity was chosen to simulate the magnitude of the rainfall experienced in the area during the typhoon Sendong in 2012, while the 30.2 mm/h intensity replicates experiential moderate rainstorms.

3. Results and Discussion

3.1 In situ Soil Data

The undisturbed samples revealed the field dry densities in the range of 846 kg/m^3 to 1,022 kg/m^3. The soil was classified as CL (strong brown sandy clay with some gravels) according to the Unified Soil Classification System (USCS). It has the following index properties: liquid limit = 40.54%, plastic limit = 11.49%, and plasticity index = 29.05%. Moreover, the soil exhibited the following textural compositions: 45.83% gravel, 17.6% sand, and 33.11% clay.

3.2 Moisture Curves

The variations in volumetric soil moisture contents (θ) with time (t) were plotted for the different surface angles (α) and depths (d). These are shown in Figure 2 for simulated rainfall intensity (r_1) of 30.2 mm/h and Figure 3 for r_2

= 50 mm/h, respectively. As shown, all curves initially followed similar patterns of gradual rise from their initial horizontal plots at θ_i up to reaching their peak slopes. However, the manner in which they continued rising to reach their respective threshold (peak) points differed according to the varied parameter α, depth d, and in particular case, r.

A distinctive character of moisture threshold attainment was observed at a depth of 0.626 m for $0° \leq \alpha \leq 20°$ (Figure 2a and Figure 3a), where the curves instantly transitioned back to horizontal plots implying a very rapid moisture increase at the impermeable boundary.
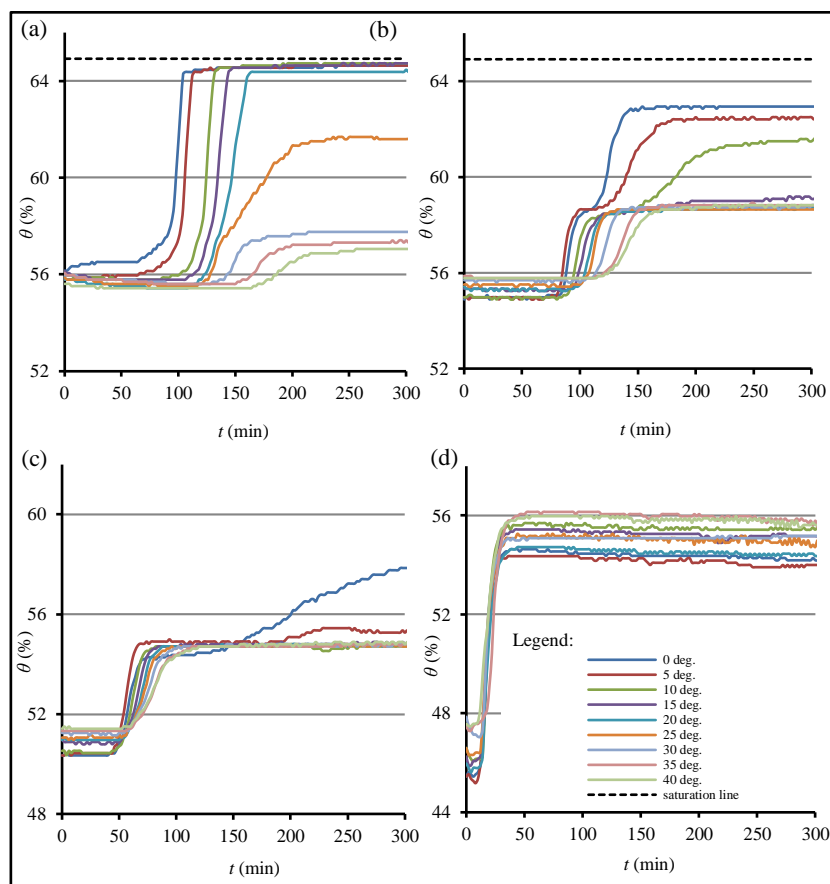

Figure 2. Variations in volumetric soil moistures (θ) with time (t) for varied surface angles (α) at depths; 0.626 m (a), 0.442 m (b), 0.258 m (c), and 0.075 m (d), for given rainfall intensity (r) of 30.2 mm/h

Because the gradients were gentle, the subsurface draining capacity of the soil was limited to the extent where water mounding at the bottom was permitted. This resulted in the development of transient water table, leading to the partial saturation of the soil. As the graphs indicate, this saturation state was only possible for the stated slope range and for both values of *r*. However, the water accumulation had triggered second-time onsets of θ escalations a few minutes after full saturation of the bottom soil. This can be evidently supported by the formation of the middle horizontal plots shown in Figures 2b, 2c, 3a, and 3b. The extent to which these developed appeared to be influenced by the parameter *r*. As shown, the higher rainfall intensity r_2 has a wider range of α (up to 20° at the height of 0.442 m) that can result in a further increase in θ than the lower intensity r_1.
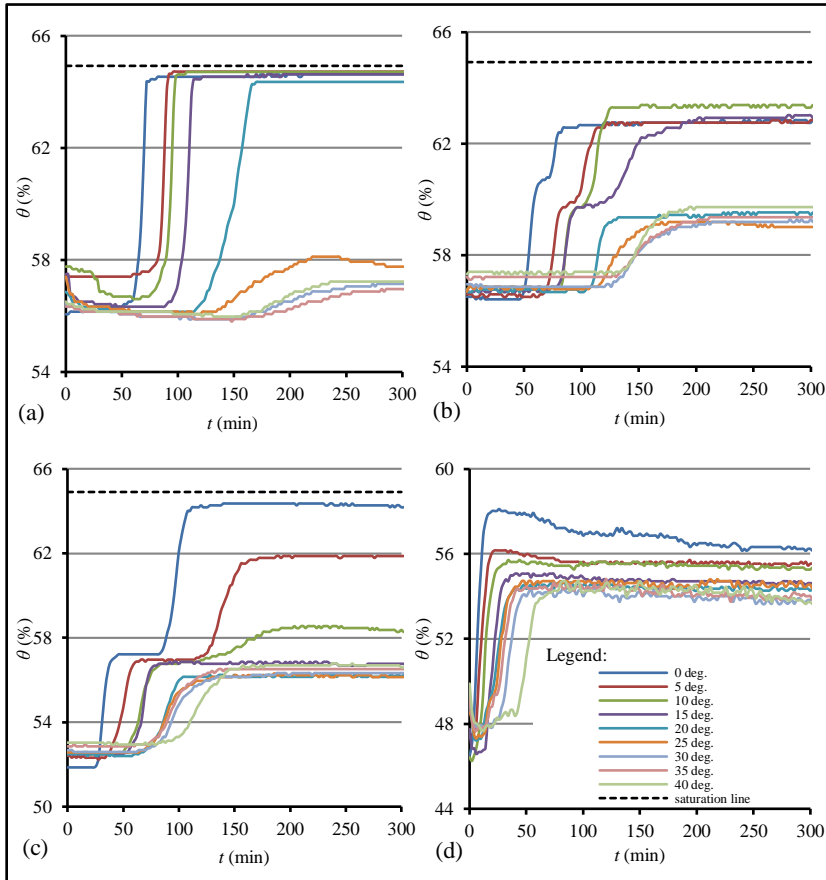

Figure 3. Variations in volumetric soil moistures (θ) with time (*t*) for varied surface angles (α) at depths; 0.626 m (a), 0.442 m (b), 0.258 m (c), and 0.075 m (d), for given rainfall intensity (*r*) of 50 mm/h

Furthermore, it can be observed that the increase in α has a delaying effect (curve translation) in the response of moisture curves, especially at greater depths. Partly, this can be attributed to the following: (1) increased surface runoff due to increased gradient resulting in reduced water volume infiltrating into the soil, and (2) increase in the effective depth (d^*) of the soil to $d^* = d / cos\alpha$. The authors also noted that the changes in the soil properties, particularly in the uppermost part (due to the cycles of wetting and drying/draining), might have intervened in the actual infiltration process.

3.3 Movement of Infiltration Front

The elapsed times (t_e) measuring the velocity (v) of the downward movement of the infiltration front are organized in Table 2 and plotted in Figure 4.

Table 2. Elapsed time for infiltration front to reach the instrumented depths

Depth (m)	Rainfall intensity, $r = r_1 = 30.2$ mm/h				time (min)				
	$\alpha = 0°$	$5°$	$10°$	$15°$	$20°$	$25°$	$30°$	$35°$	$40°$
0.075	12 ; 12	12 ; 13	16 ; 14	14 ; 14	14 ; 15	14 ; 16	16 ; 17	10 ; 19	10 ; 20
0.258	48 ; 42	46 ; 44	48 ; 47	54 ; 50	54 ; 53	56 ; 56	58 ; 60	60 ; 65	62 ; 70
0.442	82 ; 72	78 ; 76	90 ; 80	94 ; 85	98 ; 90	102 ; 96	110 ; 103	120 ; 111	120 ; 119
0.626	92 ; 103	100 ; 108	116 ; 114	118 ; 120	122 ; 128	128 ; 136	144 ; 146	168 ; 157	182 ; 169
	Rainfall intensity, $r = r_2 = 50$ mm/h								
0.075	2 ; 8	4 ; 9	6 ; 11	12 ; 13	12 ; 15	14 ; 17	20 ; 19	14 ; 22	22 ; 26
0.258	26 ; 28	36 ; 32	50 ; 37	56 ; 43	64 ; 50	66 ; 58	72 ; 67	76 ; 77	94 ; 89
0.442	44 ; 48	66 ; 56	78 ; 64	80 ; 74	104 ; 86	112 ; 99	128 ; 115	132 ; 133	138 ; 153
0.626	56 ; 68	78 ; 79	84 ; 91	92 ; 105	112 ; 122	136 ; 140	174 ; 162	180 ; 188	188 ; 217

Note: observed ; predicted

The elapsed times were reckoned from the instant the sprinkler was turned on up to the time when the sensors respectively started to register an increase in the soil moisture content. Generally, the results revealed a gentling trend in the average slope of each plot, owing to the increase in the surface slope, α. The regression analysis of the data showed the following equations as practical approximations to the $t_e - d$ relationship.

$$t_e = \begin{cases} \dfrac{d}{-6\text{x}10^{-5}\alpha + 0.0061} & ; r_1 = 30.2 \text{ mm/h} \\[2ex] \dfrac{d}{0.0092e^{-0.029\alpha}} & ; r_2 = 50 \text{ mm/h} \end{cases} \qquad (1)$$

where:

> t_e = elapsed time measured in minutes
> d = soil depth normal to the surface measured in meters
> α = surface angle from the horizontal measured in degrees

The relations given in Equation 1 suggest that the infiltration front was basically progressing downward at constant velocity as follows:

$$v = \begin{cases} -6\text{x}10^{-5}\,\alpha + 0.0061 & ;\ r_1 = 30.2 \text{ mm/h} \\[2ex] 0.0092e^{-0.029\alpha} & ;\ r_2 = 50 \text{ mm/h} \end{cases} \qquad (2)$$

Where v is the velocity component normal to the soil surface expressed in meters per minute. Equation 2 indicates a decreasing speed of the infiltration front movement with increasing α. However, when compared, the scatter plots shown in Figure 4 are more dispersed for r_2 than for r_1. This is an implication of the proportionate influence of r to the reduction in v. That is, the rate at which v decreased with increasing α had become more pronounced for the higher rainfall intensity, r_2. This behavior was captured by the steepening of the slope of the velocity curve as would be observed by direct inspection of the α coefficients in Equation 2.
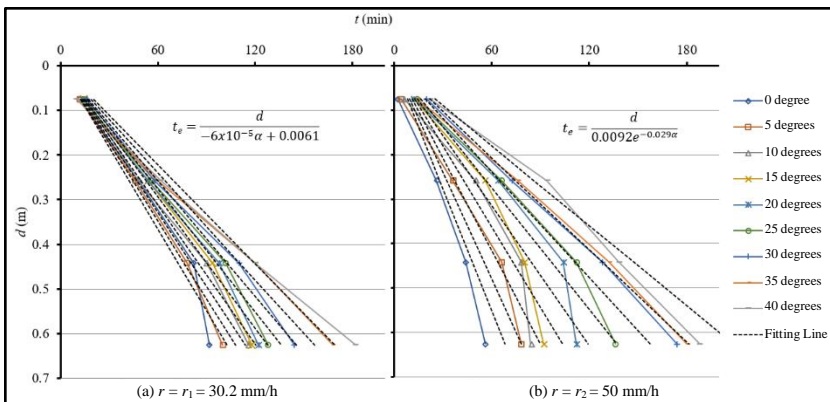

Figure 4. Scatter plots of the elapsed time against soil depth describing the infiltration front movement

Magnitude wise, v was not always faster with the higher r_2. As would be observed from the table, the relatively faster front movement with r_2 was only recorded for $0° \leq \alpha \leq 20°$. However, for steeper slopes, it became slower. Nonetheless, the difference was in no case higher than 30 min. The slowest v was observed at the steepest slope ($\alpha = 40°$). At this inclination, and for both values of r, the recorded elapsed time for the infiltration front to reach a normal depth of 0.626 m was at least 3 hours (h).

3.4 Saturation Threshold and Rainfall Duration

The highest degree of soil saturation attained by the test soil exposed to a prolonged rainfall is referred to in this paper as the saturation threshold (S_T). The corresponding time lapse for attaining this wettest soil state is then referred to as the rainfall duration. Though defined as the highest degree, the saturation threshold may not necessarily signify a fully saturated state.

The saturation threshold and rainfall duration observed at rainfall intensity of 30.2 mm/h are tabulated in Table 3. The same data are plotted in Figure 5.

Table 3. Saturation and rainfall duration thresholds at 30.2 mm/h rainfall intensity

Depth (m)	$r = r_1 = 30.2$ mm/h *Saturation Threshold S_T (%)*								
	$\alpha = 0°$	$5°$	$10°$	$15°$	$20°$	$25°$	$30°$	$35°$	$40°$
0.075	83.9	83.7	85.7	85.1	84.3	85.1	84.8	84.8	86.2
0.258	89.0	84.4	84.3	84.2	83.7	84.0	84.3	84.3	84.3
0.442	96.1	96.0	94.7	90.2	90.2	90.3	90.5	90.6	90.5
0.626	99.0	99.2	99.4	99.4	99.2	95.0	89.0	88.3	87.9
	Rainfall Duration (min)								
0.075	32	36	36	34	44	44	36	48	52
0.258	286	68	82	80	88	92	102	114	120
0.442	142	176	256	128	132	132	150	176	188
0.626	104	114	136	148	164	236	214	236	256

A fully saturated state was observed at the instrumented depth of 0.626 m (0.074 m from the bottom) for $0° \leq \alpha \leq 20°$, except that there were some amounts of trapped air that reflected a difference of no more than 1%. This means that for the slope range, partial saturation of the soil was possible. Considering the thickness tributary to the point of instrumentation, the ratio of the saturated zone to soil depth for this case can be approximated at 0.24. High values of S_T ranging from 94.7 to 96.1% observed at $0° \leq \alpha \leq 10°$ were the consequences of the second-time moisture rise due to water mounding at the bottom. For this reason, it can be seen from the table that the rainfall duration at the depth of 0.442 m for the mentioned slope range was longer than that

required to attain the threshold at the deepest point of instrumentation. In general, the results indicated a saturation threshold ranging from 83.7 to 99.4% for $0° \leq \alpha \leq 20°$ and 84.8 to 95% for steeper slopes. The highest rainfall duration was found to be no more than 4 h and 16 min for all cases of sloping surfaces.
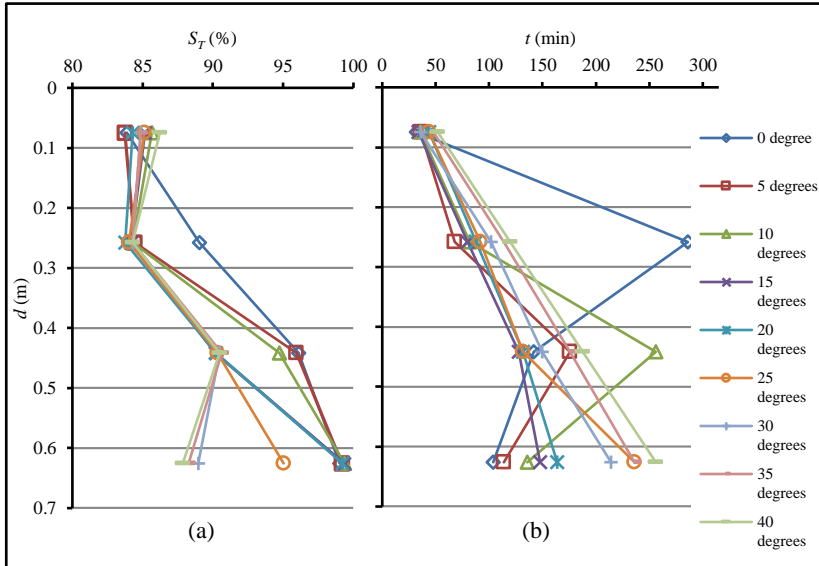

Figure 5. Scatter plots of the saturation thresholds (a) and rainfall duration (b) against soil depth at 30.2 mm/h rainfall intensity

The data obtained for the rainfall intensity of 50 mm/h are presented in Table 4 and plotted in Figure 6. The same state of partial saturation was observed, except that the saturation thresholds obtained for $0° \leq \alpha \leq 20°$ with this higher rainfall intensity were also slightly higher. Conversely, the threshold range for steeper slopes ($20° \leq \alpha \leq 40°$) was observed to be lower than those obtained with 30.2 mm/h intensity. The effect of water mounding was more pronounced reaching the depth of 0.258 m and covering an angle α of up to 15°. In effect, for $0° \leq \alpha \leq 20°$ the saturation threshold ranged from 84 to 99.7% with rainfall duration of no longer than 3 h and 24 min, while for $25° \leq \alpha \leq 40°$, the values were found at 84 to 92% with a duration of no longer than 4 h and 42 min.

Table 4. Saturation threshold and rainfall duration at 50 mm/h rainfall intensity

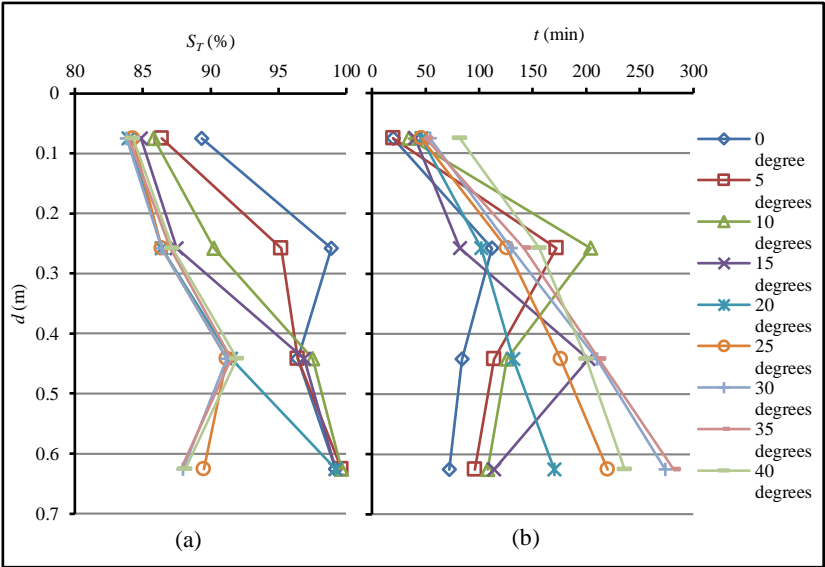| Depth (m)	$r = r_2 = 50$ mm/h	Saturation Threshold, S_T (%)							
	$\alpha = 0°$	$5°$	$10°$	$15°$	$20°$	$25°$	$30°$	$35°$	$40°$
0.075	89.3	86.4	85.8	84.9	84.0	84.3	83.8	84.0	84.3
0.258	98.9	95.2	90.3	87.5	86.4	86.4	86.4	87.0	87.2
0.442	96.4	96.4	97.5	96.9	91.5	91.2	91.2	91.5	92.0
0.626	99.2	99.7	99.7	99.2	99.2	89.5	88.0	87.8	88.1
				Rainfall Duration (min)					
0.075	20	20	34	40	46	46	54	50	82
0.258	112	172	204	82	102	126	130	142	156
0.442	84	114	126	202	132	176	210	212	200
0.626	72	96	108	114	170	220	274	282	236

Figure 6. Scatter plots of the saturation thresholds (a) and rainfall duration (b) against soil depth at 50 mm/h rainfall intensity

3.5 Implications to Slope Instability Analyses

The usual idea of assessing the occurrence probability of rainfall-induced slope instability is that the failure surface would involve a saturated zone (Godt *et al.*, 2009). The study confirmed the development of the transient water table. However, the possibility of this existence was found only for gentle slopes (less than 25°). This means that in the absence of other

intervening factors such as tension cracks, localized depressions, etc., an arbitrary assumption of the partially saturated soil state may lead to over-conservative results because slope failures usually occur at slopes steeper than the range conducive to the development of saturated zones. The rainfall duration that would bring the soil to its weakest state, which is at a saturation threshold, is practically short (less than 5 h) from the perspective of the real-time response to instability threats. Thus, the early detection of the potential hazard should be based on prior rainfall forecast rather than on the actual rainfall event to allow ample time for hazard communication and enforcement of mitigation measures.

The effective use of analytical methods for slope instability assessment necessitates the input of more precise soil moisture data. For this cause, the developed moisture charts (Figure 3) may aide in quick quantification of the degree of soil saturation. The laboratory setup, particularly the scope of instrumentation, was limited to less than a meter depth. To compensate for this limitation, the approximation of the normal movement of the infiltration front provided in Equation 2 may be coupled with the soil moisture trends from the charts to estimate the degree of saturation at greater soil depths.

4. Conclusion and Recommendation

The laboratory setup allowed the authors to replicate field slope settings and efficiently acquire data on the saturation behavior of the tested soil. The test results confirmed that the soil moisture would tend to escalate at reduced rates with an increasing slope angle. The characteristic of water infiltration responsible for moisture buildup was found to be influenced by both the slope angle and rainfall intensity. Also, higher rainfall intensity does not always signify a faster saturation rate. This observation is evident from the steepening effect of the increased rainfall intensity on the velocity curve as shown in Equation 2. Furthermore, the slope angles conducive to the development of transient water table fall within the gentle range (less than 25°), implying that the random adoption of the partially saturated soil state in analytical slope instability assessments may not always be realistic for steep slopes. Finally, the formation of a saturated zone was found to originate at the bottom of the soil then progress upwards, and an empirical equation is proposed which predicts the time required to start the formation of the saturated zone.

This investigation was limited to a controlled profile of initial soil moisture contents and bare soil surface exposure. Antecedent soil moisture is a factor that preconditions the response characteristics of soil saturation. The required amount of infiltrating rainwater to reach the soil saturation threshold is affected by the storage availability of pore spaces. Thus, the temporal character of soil saturation is also affected by the amount of moisture initially stored in the soil. Moreover, the authors preferred the bare soil surface exposure on the premise that this would yield more conservative results. However, field soils are naturally vegetated. Dense and near-surface leafy crops can create rain-shielding and surface runoff retardation effects, which are influential to rainwater infiltration and, consequently, to the saturation behavior of soil. Therefore, effect of surface vegetation is an area for further research in the future.

5. Acknowledgement

6. References

An, H., The Viet, T., Lee, G., Kim, Y., Kim, M., Noh, S., & Noh, J. (2016). Development of time-variant landslide-prediction software considering three-dimensional subsurface unsaturated flow. Environmental Modelling & Software, 85, 172-183. https://doi.org/10.1016/j.envsoft.2016.08.009

Berti, M., Martina, M.L.V., Franceschini, S., Pignone, S., Simoni, A., & Pizziolo, M. (2012). Probabilistic rainfall thresholds for landslide occurrence using a Bayesian approach. Journal of Geophysical Research, 117, 1-20. https://doi.org/10.1029/201 2JF002367

Bordoni, M., Valentino, R., Meisina, C., Bittelli, M., & Chersich, S. (2018). A simplified approach to assess the soil saturation degree and stability of a representative slope affected by shallow landslides in Oltrepò Pavese (Italy). Geosciences, 8(472), 1-18. https://doi.org/10.3390/geosciences8120472

Chen, L., & Young, M.H. (2006). Green-Ampt infiltration model for sloping surfaces. Water Resources Research, 42, 1-9. https://doi.org/10.1029/2005WR004468

Christiansen, J.E. (1942). Irrigation by sprinkling. University of California Agriculture Experiment Station Bulletin 670, Berkeley, CA.

Decagon Devices. (2018). Cover more space: ECH2O EC5. Retrieved from https://www.metergroup.com/environment/products/ec-5-soil-moisture-sensor/

Dorigo, W.A., Xaver, A., Vreugdenhil, M., Gruber, A., Hegyiová, A., Sanchis-Dufau, A.D., Zamojski, D., Cordes, C., Wagner, W., & Drusch, M. (2013). Global automated quality control of in situ soil moisture data from the International Soil Moisture Network. Vadose Zone Journal, 12(3), 1-21. https://doi.org/10.2136/vzj2012.0097

Ebel, B.A., Godt, J.W., Lu, N., Coe, J. A., Smith, J.B., & Baum, R.L. (2018). Field and laboratory hydraulic characterization of landslide-prone soils in the Oregon coast range and implications for hydrologic simulation. Vadose Zone Journal, 17(1), 1-15. https://doi.org/10.2136/vzj2018.04.0078

Farthing, M.W., & Ogden, F.L. (2017). Numerical solution of Richards' equation: A review of advances 1 and challenges. Soil Science Society of America Journal, 81(6), 1257-1269. https://doi.org/10.2136/sssaj2017.02.0058

Godt, J.W., Baum, R.L., & Lu, N. (2009). Landsliding in partially saturated materials. Geophysical Research Letters, 36(2), 1-5. https://doi.org/10.1029/2008GL035996

Green, W.H., & Ampt, G.A. (1911). Studies on soil physics. The Journal of Agricultural Science, 4(1), 1-24. https://doi.org/10.1017/S0021859600001441

Huang, C., & Yuin, S. (2010). Experimental investigation of rainfall criteria for shallow slope failures. Geomorphology, 120(3-4), 326-338. https://doi.org/10.1016/j.geomorph.2010.04.006

Lora, M., Camporese, M., & Salandin, P. (2016). Design and performance of a nozzle-type rainfall simulator for landslide triggering experiments. Catena, 140, 77-89. https://doi.org/10.1016/j.catena.2016.01.018

Montrasio, L., Valentino, R., & Quintavalla, C. (2010). Estimation of the degree of saturation of shallow soils from satellite observations to model soil slips occurred in Emilia Romagna Region of Northern Italy. International Journal of Geosciences, 1(2), 58-65. http://dx.doi.org/10.4236/ijg.2010.12008

Montrasio, L., & Valentino, R. (2016). Modelling rainfall-induced shallow landslides at different scales using SLIP - Part I. Procedia Engineering, 158, 476-481. https://doi.org/10.1016/j.proeng.2016.08.476

Muntohar, A.S., & Liao, H.J. (2008). Analysis of rainfall-induced infinite slope failure during typhoon using a hydrological-geotechnical model. Environmental Geology, 56, 1145-1159. https://doi.org/10.1007/s00254-008-1215-2

Richards, L.A. (1931). Capillary conduction of liquids through porous mediums. Journal of Applied Physics, 1(5), 318-333. https://doi.org/10.1063/1.1745010

Schilirò, L., Djueyep, G.P., Esposito, C., & Mugnozza, G.S. (2019). The role of initial soil conditions in shallow landslide triggering: Insights from physically based approaches. Geofluids, 1-15. https://doi.org/10.1155/2019/2453786

Shao, W., Bogaard, T.A., Bakker, M., & Greco, R. (2015). Quantification of the influence of preferential flow on slope stability using a numerical modelling approach. Hydrology and Earth System Sciences, 19, 2197-2212. https://doi.org/10.5194/hess-19-2197-2015

Sorbino, G., & Nicotera, M.V. (2012). Unsaturated soil mechanics in rainfall-induced flow landslides. Engineering Geology, 165, 105-132. https://doi.org/10.1016/j.enggeo.2012.10.008

Valentino, R., Montrasio, L., Losi, G.L., & Bittelli, M. (2011). An empirical model for the evaluation of the degree of saturation of shallow soils in relation to rainfalls. Canadian Geotechnical Journal, 48(5), 795-809. https://doi.org/10.1139/t10-098

White, J.A., & Singham, D.I. (2012). Slope stability assessment using stochastic rainfall simulation. Procedia Computer Science, 9, 699-706. https://doi.org/10.1016/j.procs.2012.04.075

Wu, L.Z., Zhou, Y., Sun, P., Shi, J.S. Liu, G.G., & Bai, L.Y. (2017). Laboratory characterization of rainfall-induced loess slope failure. Catena, 150, 1-8. https://doi.org/10.1016/j.catena.2016.11.002

Yu, X.N., Huang, Y.M., Li, E.G., Li, X.Y., & Guo, W.H. (2018). Effects of rainfall and vegetation to soil water input and output processes in the Mu Us Sandy Land, Northwest China. Catena, 161, 96-103. https://doi.org/10.1016/j.catena.2017.10.023